Measurement of $e^+e^- \to \eta\pi^+\pi^-$ and $e^+e^- \to \omega\pi^+\pi^-$ cross sections with the CMD-3 detector at the VEPP-2000 collider *

A.S.Popov[1,2;1)] R.R.Akhmetshin[1,2)] A.N.Amirkhanov[1,2)] A.V.Anisenkov[1,2)] V.M.Aulchenko[1,2)] V.Sh.Banzarov[1)] N.S.Bashtovoy[1)] D.E.Berkaev[1,2)] A.E.Bondar[1,2)] A.V.Bragin[1)] S.I.Eidelman[1,2)] D.A.Epifanov[1,5)] L.B.Epshteyn[1,3)] A.L.Erofeev[1,2)] G.V.Fedotovich[1,2)] S.E.Gayazov[1,2)] A.A.Grebenuk[1,2)] S.S.Gribanov [1,2;2)] D.N.Grigoriev[1,2,3)] E.M.Gromov[1,2)] F.V.Ignatov[1)] V.L.Ivanov[1,2)] S.V.Karpov[1)] A.S.Kasaev[1)] V.F.Kazanin[1,2)] A.N.Kirpotin[1)] I.A.Koop[1,2)] O.A.Kovalenko[1,2)] A.N.Kozyrev[1)] E.A.Kozyrev[1,2)] P.P.Krokovny[1,2)] A.E.Kuzmenko[1,3)] A.S.Kuzmin[1,2)] I.B.Logashenko[1,2)] P.A.Lukin[1,2)] K.Yu.Mikhailov[1)] V.S.Okhapkin[1)] A.V.Otboev[1)] Yu.N.Pestov[1)] S.G.Pivovarov[1)] G.P.Razuvaev[1,2)] A.L.Romanov[1)] A.A.Ruban[1,2)] N.M.Ryskulov[1)] A.E.Ryzhenenkov[1,2)] V.E.Shebalin[1,2)] D.N.Shemyakin[1,2)] B.A.Shwartz[1,2)] D.B.Shwartz[1,2)] A.L.Sibidanov[1,4)] P.Yu.Shatunov[1)] Yu.M.Shatunov[1)] E.P.Solodov[1,2)] V.M.Titov[1)] A.A.Talyshev[1,2)] A.I.Vorobiov[1)] Yu.V.Yudin[1)] Yu.M.Zharinov[1)]

(for the CMD-3 Collaboration)

[1] Budker Institute of Nuclear Physics, SB RAS, Novosibirsk, 630090, Russia
[2] Novosibirsk State University, Novosibirsk, 630090, Russia
[3] Novosibirsk State Technical University, Novosibirsk, 630092, Russia
[4] University of Sydney, School of Physics, Falkiner High Energy Physics, NSW 2006, Sydney, Australia
[5] University of Tokyo, Department of Physics, 7-3-1 Hongo Bunkyo-ku Tokyo, 113-0033, Japan

Abstract:

The processes $e^+e^- \to \eta\pi^+\pi^- \to \gamma\gamma\pi^+\pi^-$, $e^+e^- \to \eta\pi^+\pi^- \to \pi^0\pi^+\pi^-\pi^+\pi^-$ and $e^+e^- \to \omega\pi^+\pi^- \to \pi^0\pi^+\pi^-\pi^+\pi^-$ have been studied with the CMD-3 detector at the VEPP-2000 collider. For analysis we use data collected in the center-of-mass energy range from 1.2 to 2.0 GeV. Studied data corresponding to an integrated luminosity of 3×10^4 nb^{-1} were recorded in 2011 and 2012. The Born cross section of $e^+e^- \to \eta\pi^+\pi^-$ has been measured in the $\eta\to\gamma\gamma$ channel and is in good agreement with results obtained in other experiments. There are also preliminary results for the $e^+e^- \to \eta\pi^+\pi^-$ and $e^+e^- \to \omega\pi^+\pi^-$ Born cross sections in the $\eta \to \pi^+\pi^-\pi^0$ and $\omega \to \pi^+\pi^-\pi^0$ final states, respectively. The $e^+e^- \to \eta\pi^+\pi^-$ Born cross section data have been used to determine the $\tau^- \to \eta\pi^-\pi^0\nu^\tau$ decay branching fraction.

Key words: cross section, eta pi+ pi-, omega pi+ pi-, hadrons, branching, tau

PACS: 1–3 PACS (Physics and Astronomy Classification Scheme, https://www.aip.org/pacs)

1 Introduction

The total cross section of e^+e^- pair annihilation into hadrons can be used for the calculation of the muon anomalous magnetic moment. For this reason, we need to know all significant exclusive contributions to the $e^+e^- \to$ *hadrons* cross section. The Born cross sections of $e^+e^- \to \eta\pi^+\pi^-$ and $e^+e^- \to \omega\pi^+\pi^-$ are two examples of such exclusive channels.

Dynamics of studied processes are particularly useful for testing various phenomenological models, among them models, which allow to describe different contributions to the $\eta\pi^+\pi^-$ internal structure besides $\rho(770)\eta$. The test can be performed by studying the $\pi^+\pi^-$ invariant mass and angular distributions of final particles.

The $e^+e^- \to \eta\pi^+\pi^-$ Feynman diagram for the model of vector dominance (VDM) is shown in Fig. 1. Two of possible Feynman VDM diagrams that provide a main contribution to the process $e^+e^- \to \pi^+\pi^-\pi^+\pi^-\pi^0$ are shown in Fig. 2.

Received 14 Sep. 2014
* Supported by National Natural Science Foundation of China (55555555)
1) E-mail: aspopov1@inp.nsk.su
2) E-mail: ssgribanov@gmail.com

The result of the measurement of the $e^+e^- \to \eta\pi^+\pi^-$ can be used to find the $\eta \to \gamma^*\gamma^*$ transition form factor [1] and to test the conservation of vector current (CVC), which relates the $\tau^- \to \eta\pi^-\pi^0\nu_\tau$ decay rate with the $e^+e^- \to \eta\pi^+\pi^-$ cross section [2].

Measurements of the $e^+e^- \to \eta\pi^+\pi^-$ cross section have been also performed in the SND, BaBar and CMD-2 experiments [3, 5–11, 15]. The $e^+e^- \to \omega\pi^+\pi^-$ Born cross section measurement has been performed in the BaBar experiment [8].

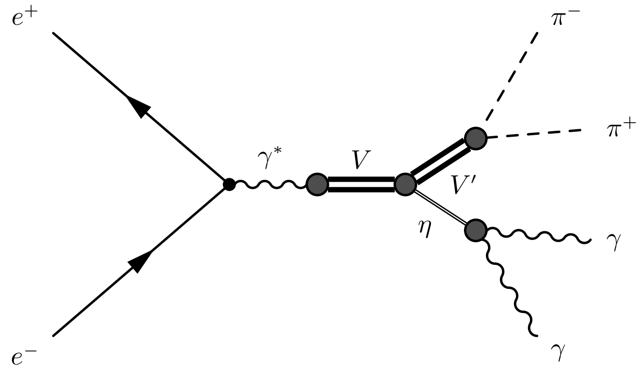

Fig. 1. Feynman diagram describing the $e^+e^- \to \eta\pi^+\pi^-$, $\eta \to \gamma\gamma$ in the vector-meson dominance model (VDM), where $V = \rho(770)$, $\rho(1450)$, $\rho(1700)$, $V' = \rho(770)$.

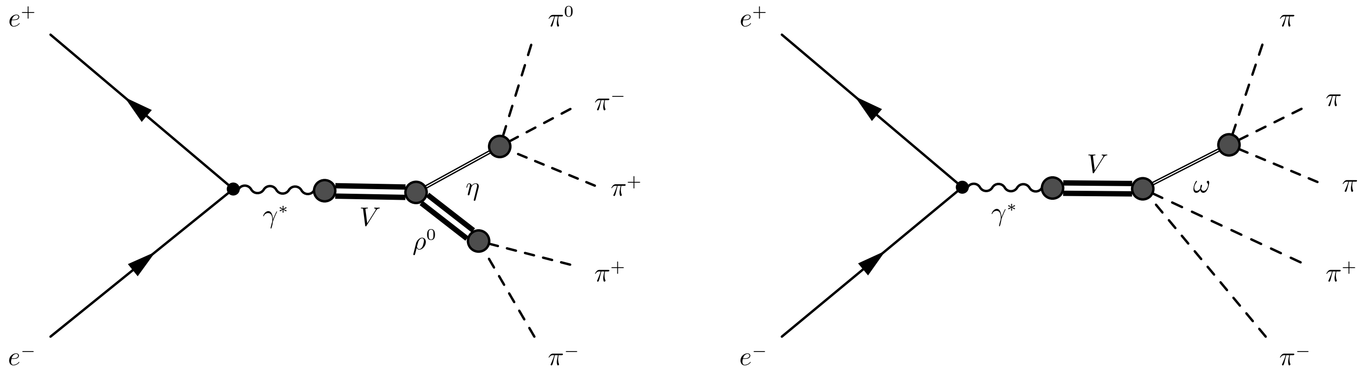

Fig. 2. Feynman diagrams of two main contributions to internal structure of the $e^+e^- \to \pi^+\pi^-\pi^+\pi^-\pi^0$ process.

2 Experiment

CMD-3 (FIG. 3) is the general-purpose cryogenic magnetic detector installed at the electron-positron collider VEPP-2000, which is situated in Budker Institute of Nuclear Physics (BINP). In order to reach the design luminosity in the single-bunch mode the round beam technique is used. This collider operates in the center-of-mass energy range from 0.32 GeV to 2.00 GeV.

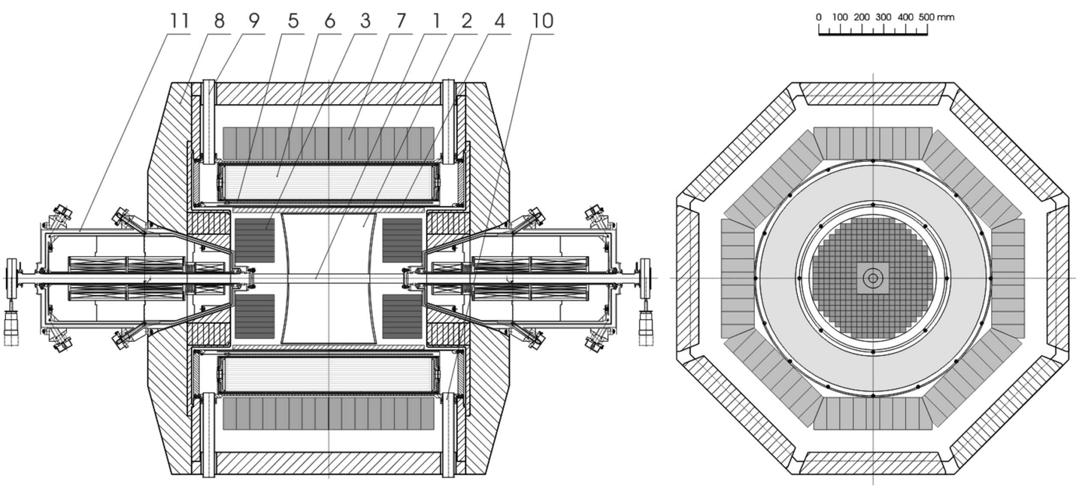

Fig. 3. CMD-3 detector. **1** - vacuum chamber, **2** - drift chamber, **3** - BGO endcap calorimeter, **4** - Z-chamber, **5** - superconducting solenoid, **6** - liquid Xe calorimeter, **7** - CsI barrel calorimeter, **8** - iron yoke, **9** - liquid He supply, **10** - vacuum pumpdown, **11** - VEPP2000 superconducting magnetic lenses

The tracking system of the CMD-3 detector consists of a double-layer multiwire proportional Z-chamber and a cylindrical drift chamber with hexagonal cells, which volume is filled with the argon-isobutane gas mixture. The magnetic field in the track system is provided by the superconducting solenoid, which surrounds the drift and Z- chambers. In 2011 the magnetic field was equal to 1.0 T and in 2012 to 1.3 T. The barrel electromagnetic calorimeter is outside of the superconducting solenoid and consists of two parts. The first part of the barrel electromagnetic calorimeter is the Liquid Xenon calorimeter ($5.4X_0$), which allows to measure the coordinates of photons with the accuracy of 1-2 mm. The second part is the CsI crystal calorimeter ($8.1X_0$). There is also the endcap BGO crystal calorimeter ($13.4X_0$), the time-of-flight and the muon system.

3 $e^+e^- \to \eta\pi^+\pi^-$, $\eta \to \gamma\gamma$

3.1 Event selection

- Each event must have at least two tracks. Furthermore, two and only two tracks must be central and have zero total charge.
- Presence of at least two photons is required.
- Bhabha background suppression. The selection criterion for track momentum noncollinearity, restriction on the energy release of two good tracks in calorimeters.
- Kinematic fit for each pair of photons. Searching the pair of photons, which gives the minimal χ^2 after a kinematic fit.
- Restriction on the χ^2 after the kinematic fit: $\chi^2 < 60$.

3.2 Simulation of the $e^+e^- \to \eta\pi^+\pi^-$ process and detection efficiency.

Simulation of the $e^+e^- \to \eta\pi^+\pi^-$ process has been performed using the Monte Carlo method. For this goal we need to know the dependence of the $e^+e^- \to \eta\pi^+\pi^-$ invariant amplitude on momenta of the final particles. This dependence has the form:

$$M_{e^+e^-\to\eta\pi^+\pi^-} \sim \frac{\epsilon_{\alpha\beta\lambda\delta} J_l^\alpha P_\eta^\beta P_{\pi^+}^\gamma P_{\pi^-}^\delta}{D_\rho(P_\rho = P_{\pi^+} + P_{\pi^-})}, \qquad (1)$$

where P_{η,π^+,π^-} are momenta of final particles, J_l is the lepton current and $D(P_\rho)$ is the inverse propagator of the $\rho-$meson.

The detection efficiency has been found using Monte Carlo simulation of $e^+e^- \to \eta\pi^+\pi^-$. To take into account track loss and differences between the simulated and experimental distributions the detection efficiency correction has been performed. The corrected detection efficiency is shown in Fig. 4.

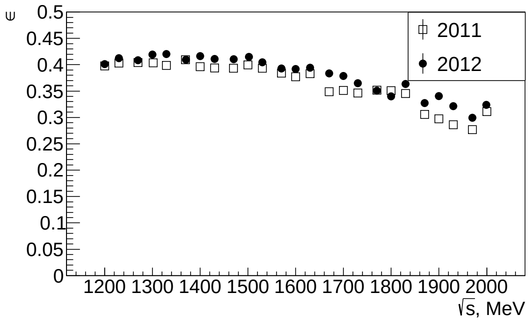

Fig. 4. Detection efficiency for the process $e^+e^- \to \eta\pi^+\pi^-$, $\eta \to \gamma\gamma$

3.3 Internal structure of the $\eta\pi^+\pi^-$ final state

The two-pion invariant mass distribution shown in Fig. 5 has a peak of the $\rho(770)$ resonance. The $\pi^+\pi^-$ invariant mass spectrum from simulation is in good agreement with the same spectrum from experiment. Simulation takes into account just the $\eta\rho(770)$ internal state. Good agreement between the $\pi^+\pi^-$ invariant mass spectra from simulation and experiment means that the $\eta\rho(770)$ internal state dominates in the $e^+e^- \to \eta\pi^+\pi^-$ process.

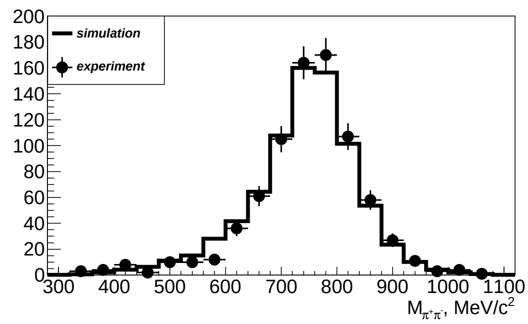

Fig. 5. The $\pi^+\pi^-$ invariant mass spectrum in the center-of-mass energy range 1475-1725 MeV with hard selection criteria: $N_\gamma = 2$, $\chi^2 < 30$. N_γ is the number of photons in an event. All other selection criteria are standard. The two π-meson invariant mass spectrum from the simulation is normalized to the number of events in the experimental spectrum.

Fig. 6 shows the distribution of the η-meson polar angle. The distribution from simulation of the $e^+e^- \to \eta\pi^+\pi^-$ process is in good agreement with the same distribution from experiment. The shape of the η-meson polar angle distributions seems to be very close to $1+cos\theta_\eta^2$.

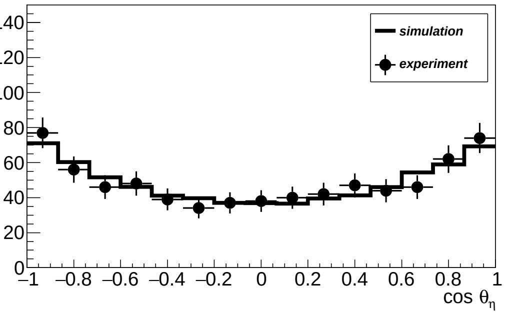

Fig. 6. Cosine of the polar angle of the η-meson in the center-of-mass energy range 1475-1725 MeV with hard selection criteria: $N_\gamma = 2$, $\chi^2 < 30$. N_γ is the number of photons in an event. All other selection criteria are standard. The distribution from simulation is normalized to the number of events in the experimental distribution.

3.4 Measurement of the $\eta\pi^+\pi^-$ event yield

Spectra of the two-photon invariant mass from simulation of $e^+e^- \to \eta\pi^+\pi^-$ have been fitted by a linear combination of normal distributions normalized to the free parameter, which gives the number of events in each simulation spectrum. The example of the fitted two-photon invariant mass spectrum for the point with the center-of-mass energy of 1500 MeV in simulation is shown in Fig. 7.

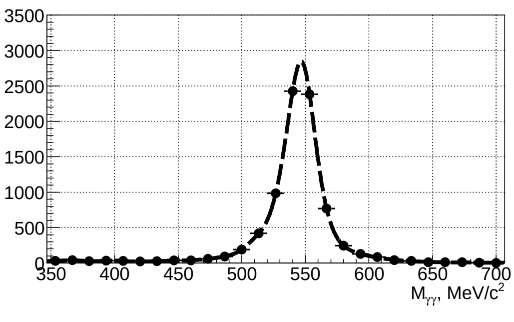

Fig. 7. Fit of the two-photon invariant mass spectrum at the center-of-mass energy of 1500 MeV of in simulation.

The experimental two-photon invariant mass spectra have been fitted by a sum of the second-order polynomial and shifted fit function from simulation with a resolution correction. All parameters in the fit function from simulation besides the number of events are fixed. The shift of the fit function from simulation along the two-photon invariant mass axis is a free fit parameter. The resolution correction dispersion and parameters of the second-order polynomial are also free. An example of the fitted two-photon invariant mass in experiment at 1500 MeV is shown in Fig. 8.

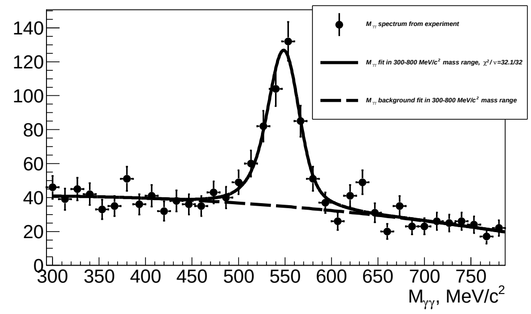

Fig. 8. Fit of the two-photon invariant mass spectrum at 1500 MeV in experiment.

3.5 Results and discussion

The visible cross section at the ith center-of-mass energy point is determined as

$$\sigma_{\mathrm{vis}}(\mathrm{E_i}) = \frac{\mathrm{N(E_i)}}{\epsilon(\mathrm{E_i})\mathrm{B}(\eta \to \gamma\gamma)\mathrm{L(E_i)}}, \tag{2}$$

where $\mathrm{E_i}$ is the ith center-of-mass energy, N is event yield, ϵ is detection efficiency, $\mathrm{B}(\eta \to \gamma\gamma)$ is branching fraction ot the $\eta \to \gamma\gamma$ decay and L is luminosity. Luminosity is measured using Bhabha scattering [12].

The relation between the visible and Born cross sections is given by the following formula [13].

$$\sigma_{\mathrm{vis}}(s) = \int\limits_0^{1-\frac{(2m_\pi+m_\eta)^2}{s}} dx\sigma_{\mathrm{B}}(s(1-x))F(x,s), \tag{3}$$

where σ_{vis} and σ_{B} are the visible and the Born cross sections, respectively, $F(x,s)$ is the ISR radiator function, m_π and m_η are masses of π-meson and η-meson, respectively. This relation is used to fit the visible cross section and get VDM parameterization parameters of the Born cross section. Then the Born cross section experimental data can be represented as

$$\sigma_{\mathrm{B}}(\mathrm{E_i}) = \frac{\sigma_{\mathrm{vis}}(\mathrm{E_i})}{1+\delta(\mathrm{E_i})}, \qquad 1+\delta(\mathrm{E_i}) = \frac{\sigma_{\mathrm{vis}}^{\mathrm{fit}}(\mathrm{E_i})}{\sigma_{\mathrm{B}}^{\mathrm{fit}}(\mathrm{E_i})}, \tag{4}$$

where σ_{vis} is the experimental visible cross section, $\mathrm{E_i}$ is the ith center-of-mass energy, δ is a radiative correction, $\sigma_{\mathrm{vis}}^{\mathrm{fit}}$ and $\sigma_{\mathrm{B}}^{\mathrm{fit}}$ are visible and Born cross section fit functions, respectively. Energy dependence of the $e^+e^- \to \eta\pi^+\pi^-$ Born cross section is shown in FIG. 9. The systematic uncertainty in the measured Born cross section is 4.3.

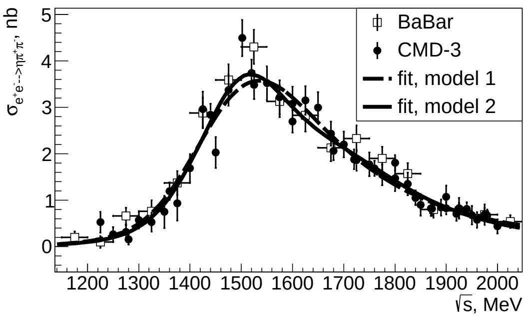

Fig. 9. The Born cross section of the $e^+e^- \to \eta\pi^+\pi^-$ process measured in the $\eta \to \gamma\gamma$ channel.

The function used for the parameterization of the $e^+e^- \to \eta\pi^+\pi^-$ Born cross section is based on the VDM model with several isovector (the isoscalar part is suppressed by G-parity conservation) contributions of the states $\rho(770), \rho(1450)$ and $\rho(1700)$ decaying to $\eta\rho(770)$ [3, 14]:

$$\begin{aligned}
\sigma_B(s) &= \int\limits_{4m_\pi^2}^{\left(\sqrt{s}-m_\eta\right)^2} \frac{d\sigma}{dq^2}(s,q^2)dq^2 \qquad (5)\\
\frac{d\sigma}{dq^2}(s,q^2) &= \frac{4\alpha^2}{3s\sqrt{s}} \frac{\sqrt{q^2}\Gamma_\rho(q^2)p_\eta^3(s,q^2)}{\left(q^2-m_\rho^2\right)^2+\left(\sqrt{q^2}\Gamma_\rho(q^2)\right)^2}|F(s)|^2\\
p_\eta^2 &= \frac{\left(s-m_\eta^2-q^2\right)^2-4m_\eta^2q^2}{4s},\\
\Gamma_\rho(q^2) &= \Gamma_\rho(m_\rho^2)\frac{m_\rho^2}{q^2}\left(\frac{p_\pi^2(q^2)}{p_\pi^2(m_\rho^2)}\right)^{\frac{3}{2}},\\
p_\pi^2(q^2) &= q^2/4-m_\pi^2,
\end{aligned}$$

where q is the momentum of the 2π system, and form factor F(s) corresponds to transition $\gamma^\star \to \eta\rho$:

$$\begin{aligned}
F(s) &= \sum_V \frac{m_V^2}{g_{V\gamma}} \frac{g_{V\rho\eta}}{s-m_V^2+i\sqrt{s}\Gamma_V(s)}, \qquad (6)\\
V &= \rho(770),\, \rho(1450),\, \rho(1700).
\end{aligned}$$

The parameters $g_{V\rho\eta}$ and $g_{V\gamma}$ are the coupling constants for the transitions $V \to \rho\eta$ and $V \to \gamma^\star$ and should be redefined as $g_{V\rho\eta}/g_{V\gamma} = g_V e^{i\phi_V}$. The coupling constants related to $\rho(770) \to \rho(770)\eta$ are calculated using data on the partial widths for the decays $\rho(770) \to e^+e^-$ and $\rho(770) \to \eta\gamma$ [3, 4]:

$$\begin{aligned}
g_{\rho\gamma}^2 &= \frac{4\pi}{3}\alpha^2\frac{m_\rho}{\Gamma(\rho\to e^+e^-)},\; g_{\rho\gamma}\approx 4.96, \qquad (7)\\
g_{\rho\eta\gamma}^2 &= \frac{24}{\alpha}m_\rho^3\frac{\Gamma(\rho\to\eta\gamma)}{\left(m_V^2-m_\eta^2\right)^3},\; g_{\rho\eta\gamma}\approx 1.59\,\mathrm{GeV}^{-1},\\
g_{\rho\rho\eta} &= g_{\rho\gamma}g_{\rho\eta\gamma}\approx 7.86\,\mathrm{GeV}^{-1}.
\end{aligned}$$

The best phase combination $\phi_{\rho770} = 0$ and $\phi_{\rho1450} = \phi_{\rho(1700)} = \pi$ was obtained and fixed in the following approximation. The parameters of the $\rho(770)$ resonane are fixed at the nominal values. The "model 1" contains free parameters $g_{\rho1450}$, $M_{\rho1450}$, $\Gamma_{\rho1450}$, but parameters $g_{\rho(1700)}$, $M_{\rho(1700)}$, $\Gamma_{\rho(1700)}$ are fixed ($g_{\rho(1700)} = 0$). The "model 2" contains free parameters $g_{\rho1450}$, $M_{\rho1450}$, $\Gamma_{\rho1450}$ and the parameters of the $\rho(1700)$ resonance are also free. The contribution of the $\rho(1700)$ obtained in the fit in "model 2" is not statisticaly significant. The value of χ^2/ν for the fit in "model 1" is 53.27/46, where ν is the number of degrees of freedom. This value corresponds to the probability $P(\chi^2,\nu) \approx 21\%$. The value of χ^2/ν for the fit in "model 2" is 50.26/43, which corresponds to the probability $P(\chi^2,\nu) \approx 21\%$.

The $e^+e^- \to \eta\pi^+\pi^-$ Born cross section can be used to calculate the $\tau^- \to \eta\pi^-\pi^0\nu_\tau$ branching fraction. To reach this goal we need to use the following formula, which has been obtained under the CVC hypothesis [3, 16].

$$\begin{aligned}
&\frac{B(\tau^-\to\eta\pi^-\pi^0\nu^\tau)}{B(\tau^-\to\nu_\tau e^-\bar{\nu_e})} = \frac{3m_\tau^2 cos^2\theta_C}{2\pi\alpha^2}\times\\
&\int\limits_0^1 dx x\left(1-x\right)^2\left(1+2x\right)\sigma_{e^+e^-\to\eta\pi^+\pi^-}(m_\tau^2x). \qquad (8)
\end{aligned}$$

Calculations performed for our $e^+e^- \to \eta\pi^+\pi^-$ Born cross section data using this formula give us the following result for the $\tau^- \to \eta\pi^-\pi^0\nu_\tau$ branching fraction

$$B(\tau^-\to\eta\pi^-\pi^0\nu^\tau) = \left(0.147\pm0.003\pm0.006\right)\%, \qquad (9)$$

which is in agreement with the world average experimental value $\left(0.139\pm0.01\right)\%$ [4], the SND CVC result $\left(0.156\pm0.004\pm0.010\right)\%$ [3] and with the CVC result $\left(0.153\pm0.018\right)\%$ for the earlier $e^+e^- \to \eta\pi^+\pi^-$ data [2]. The first uncertainty in the $B(\tau^- \to \eta\pi^-\pi^0\nu^\tau)$ branching fraction (Eq. (9)) is statistical, the second is systematic. The statistical uncertainty has been calculated in the following way. All parameters in the VDM fit function of the $e^+e^- \to \eta\pi^+\pi^-$ Born cross section have been fixed. This function has been multiplied by a free parameter, which plays the role of a relative amplitude. The cross section has been fitted by this function. The uncertainty in the value of the free parameter in the fit function is the same as a relative statistical uncertainty in the $B(\tau^- \to \eta\pi^-\pi^0\nu^\tau)$ branching fraction.

For the calculation of a systematic uncertainty in the $B(\tau^- \to \eta\pi^-\pi^0\nu^\tau)$ branching fraction the systematic uncertainty in the $e^+e^- \to \eta\pi^+\pi^-$ Born cross section (4.3%) has been used.

4 $e^+e^- \to \eta\pi^+\pi^- \to \pi^+\pi^-\pi^+\pi^-\pi^0$ and $e^+e^- \to \omega\pi^+\pi^- \to \pi^+\pi^-\pi^+\pi^-\pi^0$

4.1 Event selection

- Each event must have at least four tracks. Furthermore, four and only four tracks must be central with zero total charge.
- Presence of at least two photons is required.
- Kinematic fit for each possible photon pair combinations in $e^+e^- \to \pi^+\pi^-\pi^+\pi^-\pi^0$ hypothesis, which requires energy-momentum conservation and origination of all particles from one vertex. Searching for a pair of photons, which gives the minimal chi square $\chi^2_{5\pi}$ after a kinematic fit. Selection criterion: $\chi^2_{5\pi} < 50$.
- Restriction on the two-photon invariant mass: $90 < M_{\gamma\gamma} < 200$.
- Kinematic fit in $e^+e^- \to \pi^+\pi^-\pi^+\pi^-$ hypothesis. Selection criterion $\chi^2_{4\pi} > 300$ to suppress background from $e^+e^- \to \pi^+\pi^-\pi^+\pi^-$ process.
- Kinematic fit with $M_{\gamma\gamma} = M_{\pi^0}$ requirement, which is needed to improve resolution in the $\pi^+\pi^-\pi^0$ invariant mass spectra.

4.2 Simulation of the $e^+e^- \to \eta\pi^+\pi^-$ and $e^+e^- \to \omega\pi^+\pi^-$. Detection efficiencies.

The simulation of the $e^+e^- \to \pi^+\pi^-\pi^+\pi^-\pi^0$ process has been performed in assumption that the intermediate states corresponding to the first and the second feynman diagrams from Fig. 2 gives the dominant contribution to the $e^+e^- \to \pi^+\pi^-\pi^+\pi^-\pi^0$ process.

The detection efficiencies of the $e^+e^- \to \eta\pi^+\pi^-$ and $e^+e^- \to \omega\pi^+\pi^-$ have been determined from simulation. These detection efficiencies are shown in Fig. 10

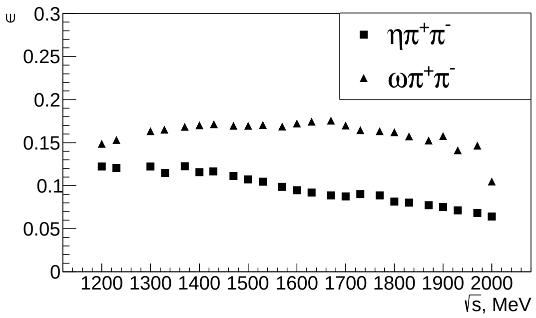

Fig. 10. Detection efficiencies for the $e^+e^- \to \eta\pi^+\pi^-$ and $e^+e^- \to \omega\pi^+\pi^-$ in $\eta \to \pi^+\pi^-\pi^0$ and $\omega \to \pi^+\pi^-\pi^0$ channels.

4.3 $\eta\pi^+\pi^-$ and $\omega\pi^+\pi^-$ event yield

The $\pi^+\pi^-\pi^0$ invariant mass spectra from simulation have been fitted using linear combination of normal distributions. The fit functions from simulation are normalized to the number of signal events.

The experimental fit function consists of fit functions from simulations of $e^+e^- \to \eta\pi^+\pi^-$ and $e^+e^- \to \omega\pi^+\pi^-$ and Gaussian background. The fit function from simulation is shifted along mass axis and has a resolution correction. Shifts and resolution corrections in each center-of-mass energy point are free parameters. All parameters in simulation besides the number of events are fixed. The $\pi^+\pi^-\pi^0$ invariant mass distribution with a fit at the point 1540 MeV is shown in Fig. 11.

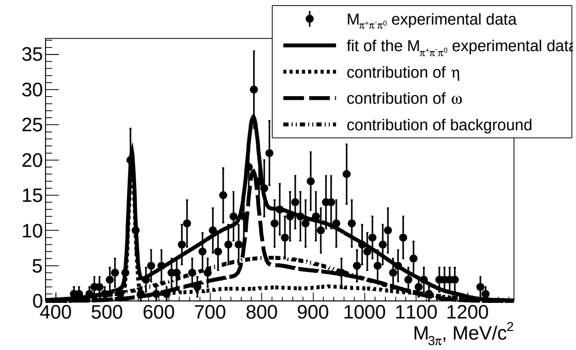

Fig. 11. $\pi^+\pi^-\pi^0$ invariant mass spectrum at 1540 MeV. $\chi^2/\nu = 127/195$, where χ^2 is chi square of the fit function and ν is the number of degrees of freedom.

4.4 Results and discussion

The Born cross sections for the $e^+e^- \to \eta\pi^+\pi^-$ and $e^+e^- \to \omega\pi^+\pi^-$ have been calculated in $\eta \to \pi^+\pi^-\pi^0$ and $\omega \to \pi^+\pi^-\pi^0$ channels, respectively, using the same technique as in the calculation of $e^+e^- \to \eta\pi^+\pi^-$ Born cross section in the $\eta \to \gamma\gamma$ channel. The results are presented in Fig. 12,13. The preliminary estimation of a systematic uncertainty for the $e^+e^- \to \eta\pi^+\pi^-$ and $e^+e^- \to \omega\pi^+\pi^-$ Born cross sections is about 10%.

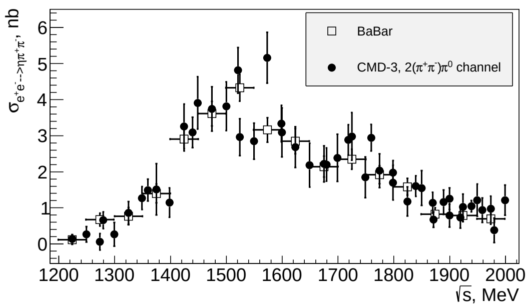

Fig. 12. The Born cross section for the $e^+e^- \to \eta\pi^+\pi^-$ process.

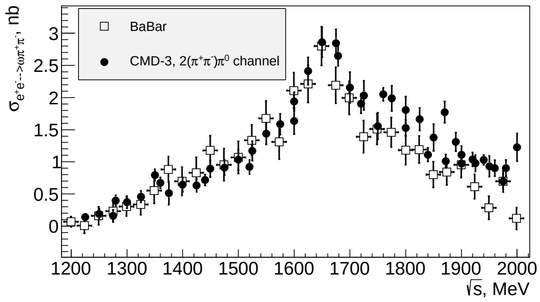

Fig. 13. The Born cross section for the $e^+e^- \to \omega\pi^+\pi^-$ process.

References

1 C. W. Xiao et al., arXiv:1509.02194 [hep-ph] (2015).
2 V. Cherepanov and S. Eidelman, Nucl. Phys. Proc. Suppl. **218**, 231 (2011).
3 V. M. Aulchenko et al. (SND Collaboration), Phys. Rev. D **91**, 052013 (2015)
4 K. A. Olive et al. (Particle Data Group) Chin. Phys. C, **3**8, 090001 (2014).
5 M. N. Achasov et al. (SND Collaboration), JETP Lett. **92**, 80 (2010).
6 M. Ablikim et al. (BES II Collaboration), Phys. Lett. B **685**, 27 (2010).
7 K. Belous et al. (Belle Collaboration), Phys. Lett. B **681**, 400 (2009).
8 B. Aubert, et al. (BaBar Collaboration), Phys. Rev. D. **76**, 092005 (2007).
9 R. R. Akhmetshin, et al. (CMD-2 Collaboration), Phys. Lett. B **489**, 125 (2000).
10 A. Antonelli et al. (DM2 Collaboration), Phys. Lett. B **212**, 133 (1988).
11 V. P. Druzhinin et al. (ND Collaboration), Phys. Lett. B **174**, 115 (1986).
12 R. R. Akhmetshin et al. (CMD-3 Collaboration), Nucl. Phys. B (Proc. Suppl.) **225-227**, 69 (2012).
13 E. A. Kuraev and V. S. Fadin Yad. Fiz. **41**, 733 (1985) [Sov. J. Nucl. Phys. **41**, 466 (1985)].
14 N.N.Achasov, V.A.Karnakov JETP Letters **3**9, 285 (1984).
15 B. Delcourt et al. (DM1 Collaboration), Phys. Lett. B **113**, 93 (1982).
16 F. J. Gilman, Phys. Rev. D **35**, 3541 (1987).